Proceedings of the 1992 IEEE/RSJ International Conference on Intelligent Robots and Systems Raleigh, NC July 7-10, 1992

A VLSI Smart Sensor for Fast Range Imaging

Andrew Gruss, Shigeyuki Tada and Takeo Kanade

School of Computer Science
Carnegie Mellon University
5000 Forbes Avenue
Pittsburgh, Pennsylvania 15213-3890

Abstract— **We have built a range-image sensor that acquires a complete 28 × 32 range frame in as little as one millisecond. Using VLSI, sensing and processing are combined into a unique sensing element that measures range in a fully-parallel fashion. The accuracy and repeatability of the sensed data is 0.1% or better. In this paper, we review the cell-parallel method used, describe our VLSI implementation, outline procedures for calibrating the cell-parallel sensor and present some experimental results. We conclude by describing a second-generation range sensor integrated circuit which is now being tested.**

I. INTRODUCTION

A cell-parallel implementation greatly improves the performance of a light-stripe range-imaging sensor[1, 2, 3]. Though equivalent to conventional light-striping from optical and geometrical standpoints, cell-parallel light-stripe sensors incorporate a fundamental improvement in the range measurement process. As a result, the acquired range data is more robust and more accurate. Furthermore, range image acquisition time is made independent of the number of data points in each frame. By fully exploiting the capability of VLSI to both sense and process information, we have built a smart sensor that acquires a complete frame of 10-bit range image data in a millisecond.

II. A CELL-PARALLEL APPROACH TO LIGHT-STRIPE RANGE IMAGING

Range information is crucial to many robotic applications. A range image is a 2-D array of pixels, each of which represents the distance to a point in the imaged scene. Many techniques for the direct measurement of range images have been developed[4]. Of these, the light-stripe methods have proven to be among the most robust and practical.

Fig. 1 illustrates the principle on which a light-stripe sensor is based. The scene to be imaged is lit by a stripe — a plane of light formed by fanning a collimated source in one dimension. The stripe is projected in a known direction using a precisely controlled mirror. When viewed by an imaging sensor, it appears as a contour which follows the profile of objects. The shape of this contour encodes range information. In particular, if projector and imaging sensor geometry are known, the distance to every point lit by the stripe can be determined via triangulation.

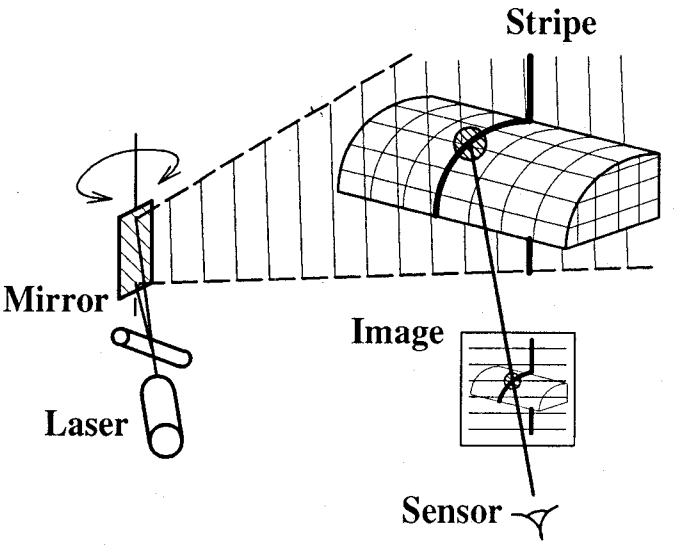

Fig. 1. Traditional light-stripe range imaging.

A conventional light-stripe range sensor builds a range image using a "step-and-repeat" procedure. A stripe is projected onto a scene, as described above, and one column of range image data is measured. The stripe is stepped to a new position and the process is repeated until the entire scene has been scanned.

Unfortunately, step-and-repeat implementations are slow. In order to build a complete range image using data from N stripe positions, N intensity images are required. The total time T_f^{Step} to acquire the range frame is

$$T_f^{\text{Step}} = NT_f^{\text{Video}}. \quad (1)$$

Assuming $T_f^{\text{Video}} = 1/30\,\text{second}$ and $N = 100$, $T_f^{\text{Step}} =$

This research was supported in part by an AT&T Foundation Grant, the National Science Foundation, under grant MIP-8915969, and the Defense Advanced Research Projects Agency, ARPA Order No. 7511, monitored by the NSF under grant MIP-9047590.

0-7803-0737-2/92$03.00 1992©IEEE

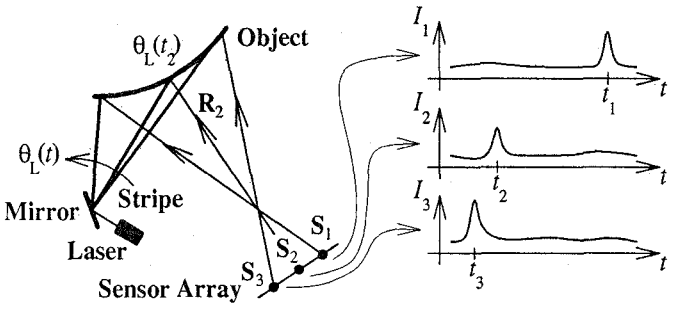

Fig. 2. Cell-parallel light-stripe range imaging.

3.3 seconds is required.

The frame time of a step-and-repeat sensor has been improved by imposing additional structure on the light source. For example, the gray-coded sources used by Inokuchi[5] reduce the factor of N in (1) to $\log_2 N$. However, achievable frame rates are still too slow and the fundamental problem remains — range frame time increases with spatial resolution.

A. The Cell-Parallel Method

The cell-parallel technique is an elegant modification of the basic light-stripe algorithm. The technique is a dynamic one, with time an important aspect of the range measurement process[6].

Consider the geometry of a three-pixel, single-row cell-parallel range sensor, seen from above in Fig. 2. In the figure, the stripe plane is perpendicular to the page. The stripe is quickly swept across the scene from right to left, briefly illuminating object features. A sensing element, say $\mathbf{S}_2$, monitors the light intensity I_2 returned to it along a fixed line-of-sight ray $\mathbf{R}_2$. When the position of the stripe is such that it intersects $\mathbf{R}_2$ at a point on the surface of an object, a "flash" will be observed by the sensing element.

Range to the object is measured by recording the *time* t_2 at which the flash is seen. The location of the stripe as a function of time is known because its projection angle $\theta_L(t)$ is controlled by the system. The "time-stamp" t_2 acquired by the sensing element measures the position of the stripe when its light is reflected back to the sensor. The three-dimensional coordinates of one object point are uniquely determined at the intersection of the line-of-sight ray $\mathbf{R}_2$ with the stripe plane at $\theta_L(t_2)$ on the surface of the object.

A sensor which collects a dense range image is formed by arranging identical sensing elements into a two-dimensional array. The cells of the array work in parallel, gathering a range image during a single pass of the light stripe. The time required to acquire the range frame is independent of its spatial resolution —

$$T_f^{\text{Cell}} = T_f^{\text{Stripe}} \tag{2}$$

The frame time T_f^{Stripe} of a cell-parallel sensor is set by the bandwidth of the photo-receptor used in its sensing elements.

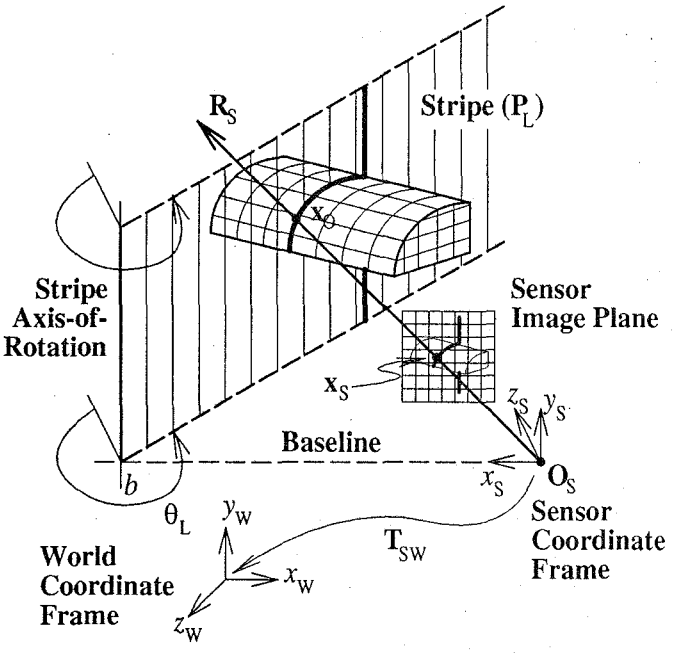

Fig. 3. Cell-parallel system geometry.

Very high frame rates ($1/T_f^{\text{Stripe}}$) can be achieved. The photodiodes used in our cell design have bandwidth into the megahertz. They can detect a stripe moving at angular velocities in excess of 6,000 rpm.

B. Cell-Parallel System Geometry

Cell-parallel system geometry can be described using homogeneous coordinate transformations[7, 8]. Referring to Fig. 3, the origin of the frame $\mathbf{O}_S$ is placed at the optical center of the imager. The stripe is a half-plane which radiates out from an axis-of-rotation aligned with the y-axis of the frame and passing through the point

$$\mathbf{x}_L = \begin{bmatrix} b & 0 & 0 & 1 \end{bmatrix}. \tag{3}$$

Stripe rotation θ_L is measured counter-clockwise about its axis when viewed from the positive y direction and defined to be zero when the stripe lies in the yz-plane. In a homogeneous representation, a plane is described in terms of a column vector $\mathbf{P}$ that satisfies the scalar product $\mathbf{xP} = 0$, where $\mathbf{x}$ is a homogeneous point that lies in $\mathbf{P}$. In the sensor coordinate frame defined above, the stripe plane is modeled in terms of b and θ_L as

$$\mathbf{P}_L = \begin{bmatrix} -\cos\theta_L \\ 0 \\ \sin\theta_L \\ b\cos\theta_L \end{bmatrix} \tag{4}$$

The position $\mathbf{x}_S = (x_S, y_S, z_S)$ of a sensing element on the sensor image plane defines the line-of-sight ray $\mathbf{R}_S$. The para-

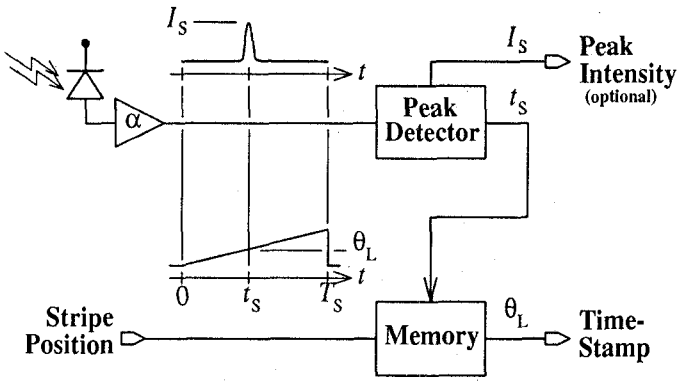

Fig. 4. Basic sensing element block diagram.

metric equation for a line in three dimensions is used to represent $\mathbf{R}_S$ as

$$\mathbf{x} = \frac{\tau}{\tau_S}(\mathbf{x}_S - \mathbf{O}_S) + \mathbf{O}_S \tag{5}$$

where $\tau_S = \|\mathbf{x}_S\| = \sqrt{x_S^2 + y_S^2 + z_S^2}$. The line parameter τ, when normalized by τ_S, is simply the distance along $\mathbf{R}_S$ measured from $\mathbf{O}_S$ heading toward the object.

The point of intersection $\mathbf{x}_O$, between the stripe and the line-of-sight, is found by solving $\mathbf{x}\mathbf{P}_L = 0$ for τ:

$$\tau = \frac{b\tau_S}{x_S - z_S \tan\theta_L}. \tag{6}$$

In the coordinate frame of the sensor, this point is

$$\mathbf{x}_O = \left[\frac{\tau}{\tau_S}x_S \quad \frac{\tau}{\tau_S}y_S \quad \frac{\tau}{\tau_S}z_S \quad 1 \right]. \tag{7}$$

Thus, the 3-D position $\mathbf{x}_O$ of imaged object points can be recovered from the scalar distance measurement τ.

III. VLSI RANGE SENSOR

A practical implementation of the cell-parallel range imaging algorithm requires a smart sensor — one in which optical sensing is local to the required processing. Silicon VLSI technology provided the means for building such a sensor.

Fig. 4 summarizes the operation of elements in the smart cell-parallel sensor array. Functionally, each must convert light energy into an analog voltage, determine the time at which the voltage peaks and remember the time at which the peak occurred.

A. A 28 × 32 *Cell-Parallel Sensor Chip*

The multi-pixel cell-parallel range sensor we have developed is shown in Fig. 5. This chip consists of 896 sensing elements arranged in a 28 × 32 array. It was fabricated using a 2 μm p-well CMOS, double-metal, double-poly process and measures 9.2 mm × 7.9 mm (width × height). Of the total 73 mm^2

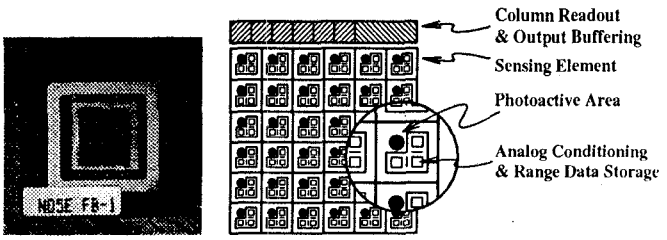

Fig. 5. Range sensor integrated circuit.

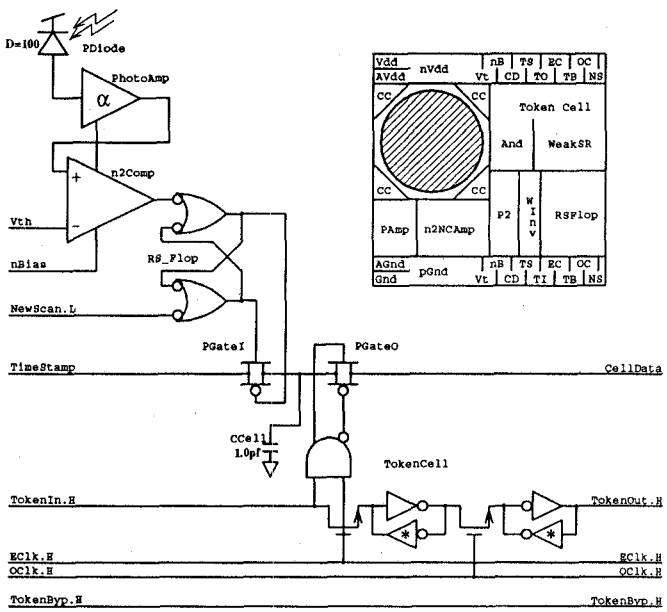

Fig. 6. Sensing element circuitry.

chip area, the sensing element array takes up 59 mm^2, read-out column-select circuitry 0.37 mm^2 and the output integrator 0.06 mm^2. The remaining 14 mm^2 is used for power bussing, signal wiring, and die pad sites.

B. *Sensing Element Design*

The architecture chosen for the range sensing elements is shown in Fig. 6. Areas of interest in the diagram include the photo-receptor (`PDiode`), the photo-current trans-impedance amplifier (`PhotoAmp`), threshold comparison stage (`n2Comp`), stripe event memory (`RS_Flop`), time-stamp track-and-hold circuitry (`PGateI/CCell`) and cell read-out logic (`PGateO/TokenCell`).

In operation, sensing elements cycle between two phases — *acquisition* and *read out*.

During the acquisition phase, each sensing element implements the cell-parallel procedure of Fig. 4. The photodiode within a cell monitors light energy reflected back from the scene. Photocurrent output is amplified and continuously compared to an external threshold voltage `Vth`. When photoreceptor output exceeds this threshold, the "stripe-detected" latch in

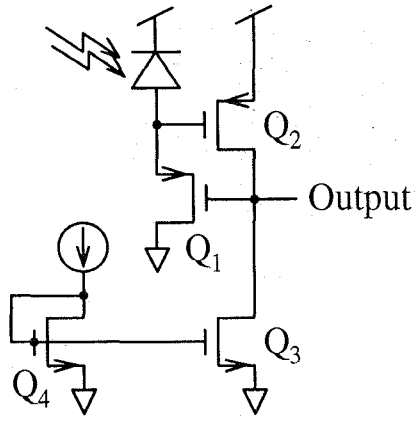

Fig. 7. Non-linear transimpedance amplifier.

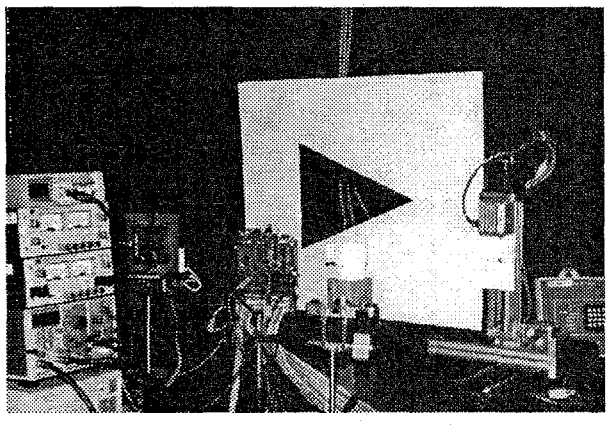

Fig. 8. The cell-parallel range-finding system.

the cell is tripped. The value of the time-stamp voltage at that instant is held on the capacitor `CCell`, recording the time of the stripe detection.

The acquisition phase is synchronized with stripe motion and ends when the stripe completes its scan. At that time, the array sensing elements recorded a range image in the form of held time-stamp values. This raw range data must now be read from the chip.

A time-multiplexed read-out scheme off loads range image data in raster order through a single chip pin. One bit of token state is passed through the sensing element array, selecting cells for output. Dual n/p-transistor pass gate structures are used throughout the time-stamp data path. They permit the use of rail-to-rail time-stamp voltages, maximizing the dynamic range of the analog time-stamp data.

C. Stripe Detection

One of the more challenging aspects of the cell design involved the circuitry which detected the stripe.

A photodiode forms the light sensitive area within each cell. This diode is a vertical structure, built using the n-substrate as the cathode and the p-well of the CMOS process as the anode. An additional p^+ implant, driven into the well, reduces the surface resistivity of the anode and increases the device bandwidth.

The non-linear transimpedance amplifier of Fig. 7 was a key element of the sensor cell design. Reflected light from the swept stripe source generates nano-amp photo-current pulses and thus a very high-gain amplifier is required to convert this current into a usable voltage. In addition, very little die area could be devoted to photo-current amplification if cell area was to be kept small. The three transistor amplifier design of Fig. 7 satisfies both requirements. Its logarithmic transfer characteristic provides freedom from output saturation even when input light levels vary over several orders of magnitude. The output rise-time of photodiode/amplifier test structures in response to a stripe was measured to be a few microseconds.

TABLE I
CELL-PARALLEL SENSOR SYSTEM SUMMARY

Baseline	300 mm	
Laser Source	Laser Diode (Collimated)	
	Wavelength	780 nm
	Output Power	30 mW
	Stripe Width	1 mm
	Stripe Spread	40° (3 dB)
Sweep Assembly	Rotating Mirror	
	Sweep Angle	40°
Sensor Optics	1/2"-Format CCD Zoom Lens	
	Focal Length	12.5 to 75 mm
	f-number	$f/1.8$
A/D Precision	12 bits	

D. Analog Signal Processing

Analog signal processing techniques played an important role in the design of this smart sensor. As shown in Fig. 6, sensing elements use analog circuitry to amplify the photo-current, to detect the stripe and to record the per-cell time-stamp information. Stripe timing is represented in analog form as a 0-5 V sawtooth broadcast to all cells of the array. This allowed the time-stamp value to be stored as charge on the 1 pf capacitor within each cell. The digital equivalent of latching a count into a multi-bit register would be significantly larger in area and would require that the digital time-stamp counters run during the acquisition phase. Thus, analog processing kept cell area small and minimized digital switching noise during photo-current measurements in the acquisition phase.

IV. PROTOTYPE RANGE IMAGE SENSOR

The 28 x 32 element VLSI sensor prototype described in the previous section was incorporated into the light-stripe range system shown in Fig. 8. System components visible in the photograph include (from the left) the stripe generation assembly,

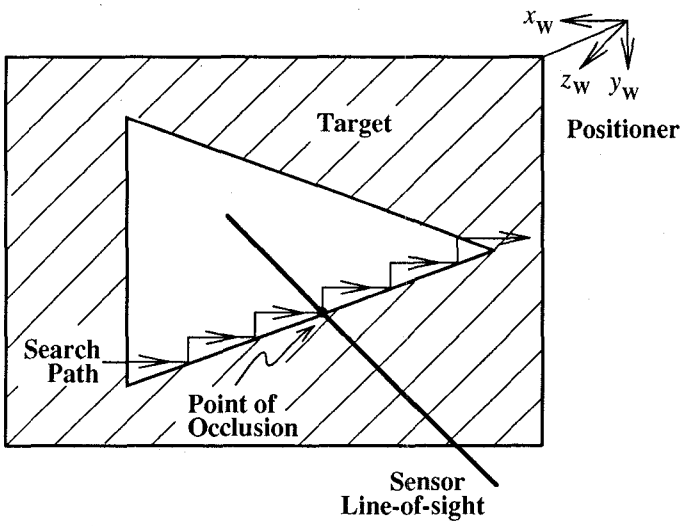

Fig. 9. Line-of-sight measurement.

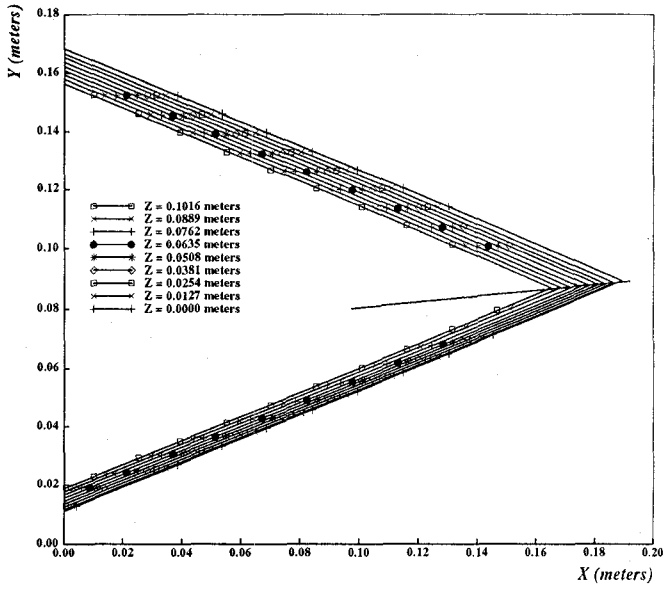

Fig. 10. Cell (13,15) measured line of sight.

the VLSI sensor chip and its interface electronics, a calibration target and the 3-DOF positioning system. Table I provides details of the configuration shown.

V. CELL-PARALLEL SENSOR CALIBRATION

Calibration provides the complete specification of system geometry necessary for converting cell time-stamp data into range images. Two sets of calibration parameters must be measured. First, 3-D sensor chip geometry and optical parameters must be measured — the *imager model*. Next, a mapping between time-stamp values θ_S and distance r for all sensing elements is developed — the *stripe model*.

A. Imager Model Calibration

This method measures component model geometry using reference objects, manipulated in the sensor's field of view with an accurate 3-DOF (degree of freedom) positioning device. The following two-step procedure is used (Fig. 3):

- the line-of-sight rays $\mathbf{R}_S$ for a few cells are measured, and
- a pinhole-camera model is fit to measured line-of-sight rays in order to approximate line-of-sights for all sensing elements.

A planer target out of which a triangular hole has been cut as shown in Fig. 9 is used to map out sensing element line-of-sight rays. The target is mounted on the positioner so that its surface is parallel to the world-xy plane.

A single 3-D point on the line-of-sight of a particular sensing element is found as follows. The target is moved to some z-position in world coordinates and held. The bottom edge of the triangular hole is located by moving the target around in x and y as indicated in Fig. 9. When a small motion in either x or y causes a large change in the time-stamp value reported by the cell, occlusion of the line-of-sight at an edge of the triangular cut is indicated.

Once many points along the bottom edge are located, a line, known to lie in the plane of the target, is fit. The location of the top edge is found in a similar fashion. The intersection of the top and bottom edge lines define one 3-D point that lies on the cell's line-of-sight. A number of these points are located by moving the target in z and repeating the process. The line-of-sight for a single cell can then be identified by fitting a 3-D line to these points. Experimental data from the calibration of one sensing element's line-of-sight is shown in Fig. 10.

Mapping the line-of-sight rays for all 896 sensing elements in this manner is too time consuming. In practice, line-of-sight information is measured for 25 cells, evenly spaced in a 5 grid. The geometry of the remaining cells is approximated using a pinhole-camera model.

The pinhole-camera model[11] constrains all sensing element line-of-sight rays to pass through a single point focus of expansion at the optical center of the camera. Fig. 11 graphically illustrates the process. Sensing element locations are assumed to lie in some *sensor plane*, at locations evenly spaced in a 2-D grid on the plane. Eleven model parameters must be determined that identify the transformation matrix $\mathbf{T}_{SW}$ and the geometry of the the sensor plane. A least-squares procedure is used to fit pinhole-model parameters to line-of-sight information measured in the first calibration step. Imager model geometry is now fully calibrated.

B. Advanced Imager Model Calibration

Unfortunately, calibration of the imager model via line-of-sight measurement is not suitable for use outside of the labo-

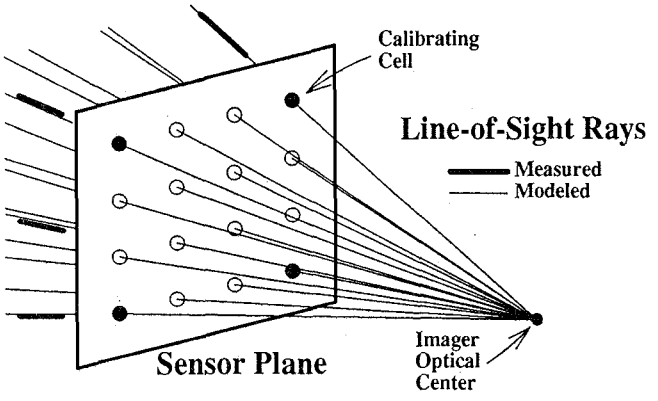

Fig. 11. "Pinhole" line-of-sight approximation.

ratory environment. "One-at-a-time" measurement of sensing element geometry, as outlined above, is slow and cumbersome.

We are developing a faster, more precise method for imager model calibration. In this new calibration method, the 3-DOF positioning system is replaced with a liquid crystal display (LCD) mask that need only be accurately positioned along one degree of freedom. The LCD mask is used to define precise black-and-white images that are "seen" by the range sensor. The method relies on intensity image information, measuring geometry through analysis of reference object images[9].

The LCD mask is placed between a diffuse planer target and sensor chip at a known position and is backlit by shining the system stripe source on the planer target. The pattern displayed on the LCD forms a black-and-white image on the sensor. Only illuminated sensing elements will latch the stripe-detected condition (Section III-B). A single-bit intensity image is derived by identifying the time-stamp output of illuminated sensing elements.

Sensing element line-of-sight geometry is found by varying the LCD mask pattern in a controlled fashion. For example, a circular pattern, whose 3-D center is known, can be projected. A calibration point is found by measuring the 2-D location of this circle's center in the intensity image returned by sensor. Additional calibration data is measured by varying the position of the circle on the LCD mask and the position of the LCD along z_S. Also, by measuring the center different radii of the circle at a fixed position, we can compensate for the low spatial resolution of the current sensor. The new sensor chip design, discussed in Section VII, returns multi-bit intensity image data which further assists imager geometry calibration.

Use of the LCD mask significantly reduces the time required to perform imager-model calibration. In the previous method, two edges of a triangular hole had to be mapped out, via accurate back-and-forth movement, in order to yield a single calibration point. In the new method, one calibration point is measured from a single LCD-generated pattern without mechanical X-Y movement. Precise calibration of the low-spatial resolution range sensor is possible because high-precision patterns are

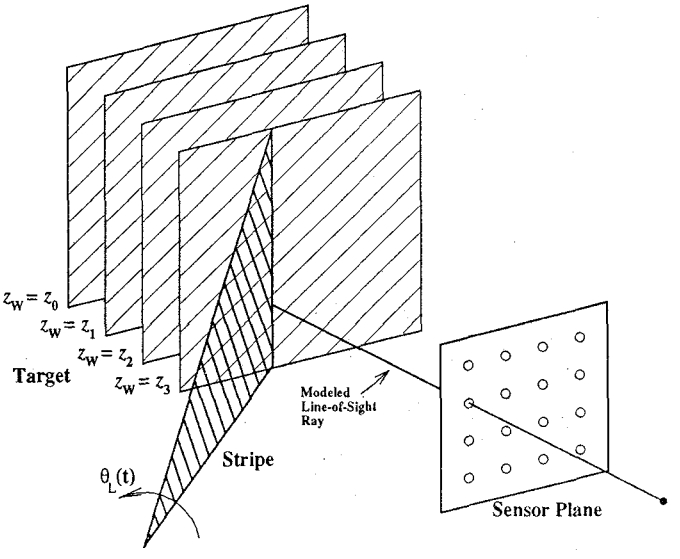

Fig. 12. Time-stamp calibration.

generated by the LCD mask.

The use of an LCD mask to project precise 2-D patterns has application beyond the calibration of our light-stripe range sensor. For example, this technique could be used to assist more traditional camera calibration procedures or to present training data to image-based neural net systems. LCD displays have several advantages over CRT displays for applications like these — they are fast, they are static (not refreshed), and they form images which are stable and well defined.

C. Stripe Model Calibration

The second part of the calibration procedure determines the mapping between time-stamp data and range along all sensing element line-of-sight rays. As shown in Fig. 12, a planer target with no hole replaces the target used in step one. The new target is held at a known world-z position, parallel to the xy plane, and time-stamp readings θ_S from all sensors are recorded. This process is repeated for many z positions. Using this information, the function which maps cell time-stamp values θ_S into line-of-sight distance r for each sensing element is approximated by fitting a parabola to each. Experimental data, showing the fitted r verses θ_S functions for several sensing elements, is shown in Fig. 13. Calibration of the cell-parallel range sensor is now complete.

VI. SYSTEM PERFORMANCE

A. Range Accuracy and Repeatability

The quality of the range data produced by the cell-parallel range sensor was measured by holding a planer target at a known world-z position with the 3-DOF positioning device. In the experimental setup, the world-z axis heads almost directly

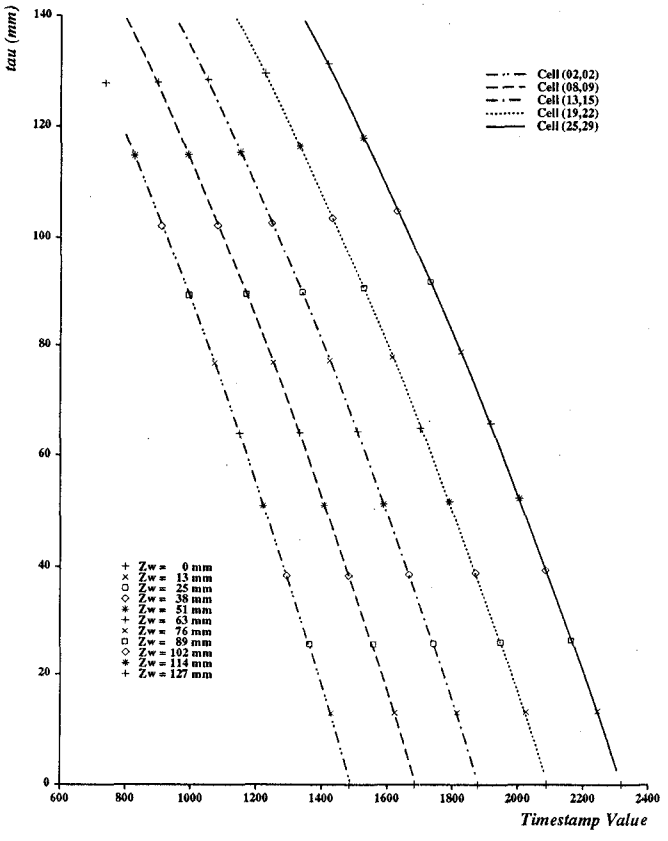

Fig. 13. Time-stamp calibration result.

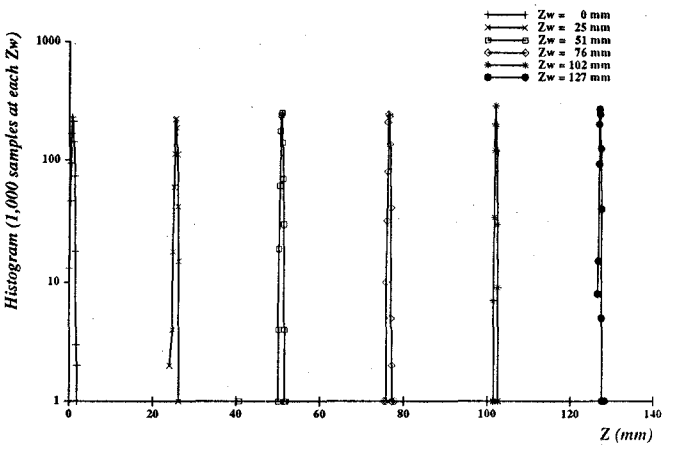

Fig. 14. Cell (13,15) range-data histograms.

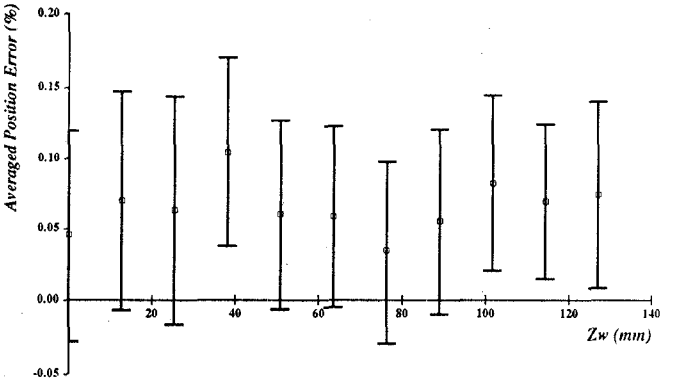

Fig. 15. Range data accuracy and repeatability.

toward the sensor with the $z_W = 0$ point roughly 500 mm away. Analog time-stamp values from the sensor array were digitized, using a 12-bit analog-to-digital converter (A/D), and recorded for 1,000 trials. Light-stripe sweep (acquisition phase) time for each scan was 3 msec.

A histogram of the range data reported by one cell is plotted in Fig. 14. The horizontal axis represents the digitized time-stamp value, converted to world-z distance via the calibration model. Data for six world-z positions are combined in this plot. The vertical axis shows the number of times (plotted logarithmically), out of the 1,000 trials, that the sensing element reported that world-z distance. The sharpness of each peak is an indication of the stability (repeatability) of the range measurements.

Averaged statistical data for 25 evenly-spaced sensing elements is plotted in Fig. 15. In order to measure accuracy and repeatability, the position of the target, as reported by the cell-parallel sensor, is compared to the actual target z position. The "boxed" points in the plot represent the mean absolute error, expressed as a fraction of the world-z position and averaged for the 25 elements at z_W. One standard deviation of "spread", also normalized with z_W, is shown (⊞) above and below each

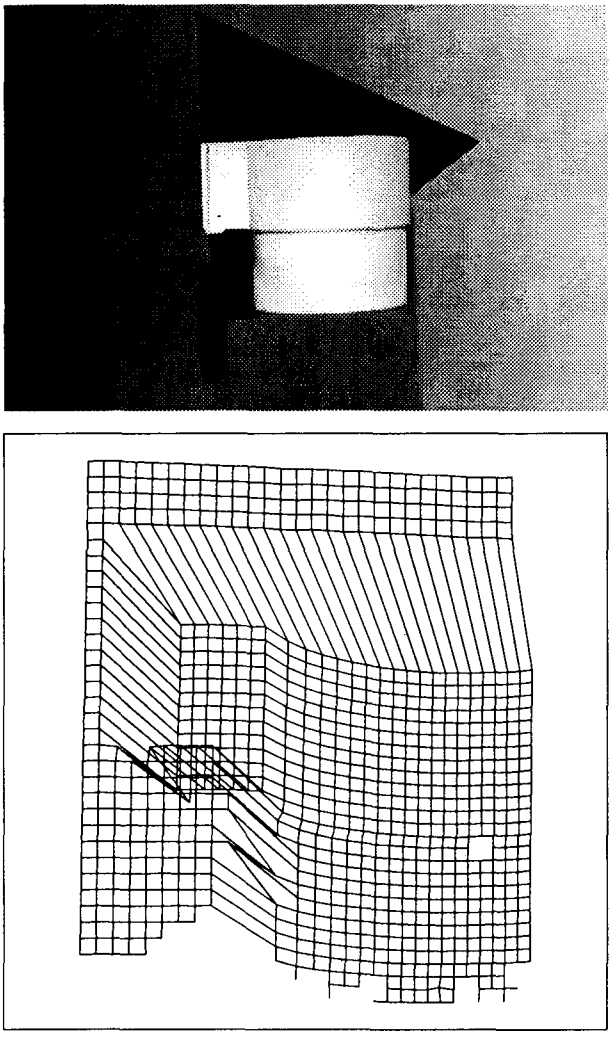

Fig. 16. Range data wire frame.

box.

The experiments show the mean measured range value to be within 0.5 mm at the maximum 500 mm z — an accuracy of 0.1%. The aggregate distance discrepancy between world and measured range values remains less than 0.5 mm over the entire 360 mm to 500 mm z range. The cell-parallel sensor repeatability is found by computing the standard deviation of the distance measurements. The measured repeatability of histogram data is less than 0.5 mm — 0.1% at the maximum 500 mm positioner translation. The 0.5 mm repeatability decreases with the distance to the sensor — essentially with the slope of the time-stamp to distance mapping function (Fig. 13).

B. Range Image Acquisition

Fig. 16 shows a wire-frame representation of one 28 × 32 range image produced by the sensor. The imaged object is the cup shown in the figure, approximately 80 mm in diameter at its opening and 80 mm high. The range sensor is looking directly at the object from a distance of 500 mm. The viewpoint of the plot is at a point directly above the optical center of the sensor. The complete range image was acquired during a 3 msec stripe scan. The intersection points of the wire-frame plot are positioned on cell line-of-sight rays at the measured distance along the ray and the focus of expansion is located in front of the cup. Thus, the smaller "squares" represent object surface patches closer to the sensor. This is opposite the manner in which straight perspective would make an object with a grid painted on it appear, and at first glance gives the false impression that the "mold" used to make the cup has been imaged.

The curved smooth front surface of the object is clearly visible in the range data. The 20 mm handle of the cup is readily distinguished, as is the planer background behind the cup. The curved surface of the object halfway down the cup directly across from the bottom of its handle includes a slight shift of the wire-frame. The imaged cup is slightly narrower at its base by about 2 mm. The cell-parallel sensor is measuring this small 3-D feature at the 500 mm object distance.

TABLE II
CELL-PARALLEL SENSOR PERFORMANCE SUMMARY

Spatial Resolution	28 × 32
Frame Time	Up to 1 msec
Operating Distance	350 to 500 mm
Accuracy	< 0.5 mm
Repeatability	< 0.5 mm

C. Sensor Performance Summary

A summary of the cell-parallel sensor system performance is given in Table II.

VII. A SECOND GENERATION SENSING ELEMENT

A second-generation implementation of the light-stripe sensor array has been fabricated. This new chip, seen in Fig. 17, incorporates several advantages over the first design. The die area of the new cell, shown in Fig. 18, is 216 μm × 216 μm, 40% smaller than that of the cells of the first-generation sensor (photoreceptor area has been kept constant). Stripe detection is done in a more robust manner and range data read-out circuitry has been simplified. In addition, the new cell provides a means to record and read out the value of the peak intensity seen when it acquires a range data sample. The peak intensity information provides a direct measure of scene reflectance because stripe output power is known and distance to the object point is measured. In addition, the availability of intensity information allows for efficient sensor calibration (Section V-B).

Peak detection is done using the circuit of Fig. 19. Operation of the circuit is straightforward. The source following transistor $\mathbf{Q}_p$ enables capacitor $\mathbf{C}_I$ to track the rising intensity input

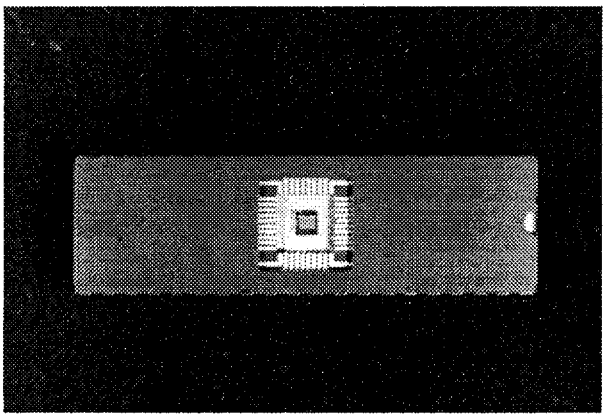

Fig. 17. Second-generation range sensor integrated circuit.

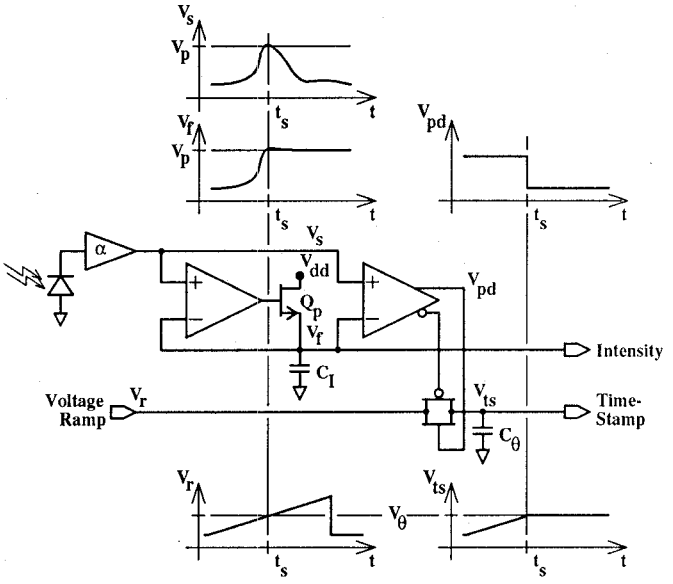

Fig. 19. Second-generation sensing element circuitry.

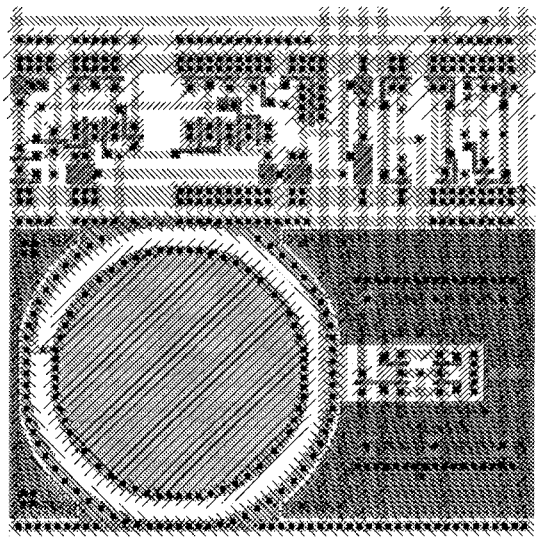

Fig. 18. Second-generation sensing element layout.

voltage transitions. No path is provided for $\mathbf{C}_p$ to discharge when photoreceptor output transitions downward. At the end of a scan, the largest intensity reading observed will be held. Stripe detection is easily accomplished by comparing the peak-intensity value $\mathbf{V}_f$ with the amplified photodiode output $\mathbf{V}_s$. When $\mathbf{V}_s$ falls below the $\mathbf{V}_f$, the output from the comparator is used to record a time-stamp value.

Using *Spice*[10], operation of of the second-generation sensing element design was simulated. The simulation results are plotted in Fig. 20. The output from the peak-following circuit `XLSCELL.30` acts as a dynamic threshold for each cell, replacing the externally applied global threshold of the first-generation design (Section III-B). Comparator input offset mismatch made setting a global threshold level, valid for all cells in the array, difficult. Thus, stripe detection is made more robust by this modification. In addition, the "true" peak detection of the new design provides better quality range data because the new stripe detection scheme identifies the location of the peak in time more accurately than simple thresholding.

The peak-intensity value held within the second-generation cell is an important artifact of the ranging process and, in the new design, is provided as an additional sensing element output. The illumination source in the system, the stripe, is of known power. Intensity reduction from $1/r$-type losses can be accounted for because range to the object is measured. The intensity value therefore provides a direct measure of scene reflectance properties at the stripe wavelength. It is an image aligned perfectly with range readings from the cell array.

The area in each cell dedicated to time-stamp read out is much smaller in the new design. Direct addressing of the cell to be read, using row and column selects, eliminates the token state necessary in the first-generation design. The $N \times M$ array

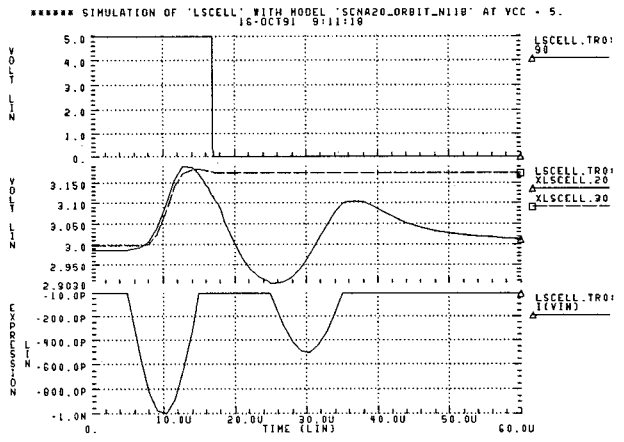

Fig. 20. Second-generation sensing element simulation result.

is read using N row select lines and M column select lines. A given cell is enabled for read out by asserting the row and column select lines that correspond to the location of the cell in the array. The two-level bus hierarchy has been maintained, however, to keep bus loading at a minimum. The area savings of the new read selection method has made cell area of the second-generation design smaller despite the additional peak detection circuitry.

VIII. CONCLUSION

We have presented the design and construction of a very high-performance range-imaging sensor. This sensor acquires a complete 28×32 range-data frame in a few milliseconds. Its range accuracy and repeatability were measured to be less than 0.5 mm on average at half-meter distances. The success of this implementation can be attributed to the use of a VLSI smart sensor methodology that allowed a practical implementation of the cell-parallel technique.

While the advantages of processing at the point sensing have been advocated by many, few practical smart-sensor implementations have been demonstrated. The cell-parallel range imager presented here bridges the gap between smart sensor theory and practice, demonstrating the impact that the smart sensor methodology can have on robotic perception systems, like automated inspection and assembly tasks.

Smart VLSI-based sensors, like the high-speed range image sensor presented here, will be key components in future industrial applications of sensor-based robotics.

REFERENCES

[1] A. Gruss, *A VLSI Smart Sensor for Fast Range Imaging*. PhD thesis, Carnegie Mellon University, November 1991.

[2] T. Kanade, A. Gruss, and L. R. Carley, "A very fast VLSI rangefinder," in *Proceedings of the 1991 IEEE International Conference on Robotics and Automation*, (Sacramento, CA), pp. 1322–29, April 1991.

[3] A. Gruss, T. Kanade, and L. R. Carley, "Integrated sensor and range-finding analog signal processor," *IEEE Journal of Solid-State Circuits*, vol. 26, pp. 184–191, March 1991.

[4] P. J. Besl, "Range imaging sensors," Research Publication GMR-6090, General Motors Research Laboratories, March 1988.

[5] S. Inokuchi, K. Sato, and F. Matsuda, "Range imaging system for 3-D object recognition.," in *Proceedings of 7th International Conference on Pattern Recognition*, (Montreal, Canada), pp. 806–808, July 1984.

[6] K. Araki, Y. Sato, and S. Parthasarathy, "High speed rangefinder," in *Optics, Illumination, and Image Sensing for Machine Vision II*, vol. 850, pp. 184–188, SPIE, 1987.

[7] D. H. Ballard and C. M. Brown, *Computer Vision*. Prentice-Hall, Inc., 1982.

[8] W. M. Newman and R. F. Sproull, *Principles of Interactive Computer Graphics*. McGraw-Hill Book Company, 2nd. ed., 1979.

[9] M. D. Altschuler, K. Bae, B. R. Altschuler, J. T. Dijak, L. A. Tamburino, and B. Woolford, "Robot vision by encoded light beams," in *Three-Dimensional Machine Vision* (T. Kanade, ed.), Kluwer Academic Publishers, 1987.

[10] Meta-Software, Inc., 1300 White Oaks Road, Campbell, CA 95008, *HSPICE User's Manual*, h9001 ed., 1990.

[11] J. Weng, P. Cohen, and M. Herniou, "Calibration of stereo cameras using a non-linear distortion model," in *Proceedings of the 10th International Conference on Pattern Recognition*, (Atlantic City, NJ), pp. 246–253, IEEE Computer Society Press, June 1990.